

# Exploiting the combined dynamic and geometric phases for optical vortex beam generation using metasurfaces

Jialong Cui, Chen Qing, Lishuang Feng, and Dengke Zhang\*

*School of Instrumentation and Optoelectronic Engineering, Beihang University, Beijing 100191, China*

The generation of optical vortex beams is pivotal for a myriad of applications, encompassing optical tweezing, optical communications, and quantum information, among others. The metasurface-based approach has realized significant advancements in vortex production, utilizing either dynamic or geometric phases. The dynamic design exhibits indifference to the polarization state of incident light, while the geometric design is inextricably tied to it. In the study, we put forth the proposition that combining dynamic and geometric phases could unlock the potential of metasurface design in generating optical vortices. A hybrid design that harnesses the combined dynamic and geometric phases can attain the same objective while offering tunable functional control over the polarization of light. We establish a correlation between the structural parameters of metasurface and the topological charge of the resulting vortices. The experimental results fully demonstrate the design's flexibility and its effective control over the polarization constraints of incident light. Our research uncovers the capacity for vortex generation through the manipulation of hybrid phases introduced by metasurfaces, indicating significant potential for the design of optical devices and the future advancement of innovative optical applications.

## I. INTRODUCTION

Optical vortex beams are typically paraxial beams characterized by their cylindrical symmetric propagation. Notably, the vortex beam's center is a dark core, where the intensity is nonexistent and remains so throughout its propagation [1, 2]. The wavefront of vortex beams exhibits a spiral-shaped distribution, resulting in its wavevector with an azimuthal component. Consequently, due to the transverse spatial phase distribution, photons acquire orbital angular momentum (OAM) [3–5]. Owing to these characteristics, vortex beams offer distinct advantages in various fields, including optical trapping, quantum entanglement, nonlinear optics, optical processing, and high-resolution microscopic imaging [2, 6]. In practical applications, vortex beams can be produced directly using active vortex laser generators [7, 8], or more commonly, by utilizing external discrete optical elements to facilitate conversion [9]. However, the optical components utilized in these techniques are bulky and non-planar, presenting challenges for optical integration in various applications.

A metasurface is an artificial material comprised of single or multiple sub-wavelength nanostructural units, strategically arranged to perform specific functions [10–12]. By carefully designing the geometry and composition of the nanostructural unit, one can effectively control the polarization state, amplitude, and phase of a light wave at a sub-wavelength scale [13–15]. The introduction of metasurfaces enables the manipulation of light fields by incorporating helical wavefronts that are phase-varied with respect to the azimuthal angle. This manipulation endows the beam with an orbital angular momentum,

thereby facilitating its transformation into an optical vortex. Incorporating metasurfaces into the engineering of optical vortex generation devices not only satisfies current requirements for miniaturization, portability, and precise polarization control but also substantially overcomes the constraints inherent in conventional vortex-generating techniques.

Utilizing metasurfaces, the helical wavefront is generated by introducing a spiral spatial phase shift through various nanostructural units [16–18]. The optical light will invariably experience a phase shift as it passes through these nanostructural units, which can be precisely manipulated by design. Theoretically, the phase shift of an optical beam can be decomposed into two distinct components: the dynamic phase and the geometric phase [19, 20]. The dynamic phase denotes the phase retardation induced by the optical element as a consequence of the beam's propagation. This phase shift is independent of the polarization or spin states of the light, being primarily influenced by the frequency of the incident light and the refractive index of the material [21]. Given that the structural thickness of nano units typically falls below the operating wavelength, the modulation of the dynamic phase is predominantly accomplished by altering the geometric dimensions or the spacing of the nano units, which in turn modifies the effective refractive index. The geometric phase originates from the interaction between spin angular momentum and OAM, exhibiting a significant dependence on the polarization state of the incoming light [22, 23]. In metasurface design, the geometric phase is frequently induced by rotating anisotropic nano units tailored for circularly polarized light [18, 24]. The two distinct types of phases have significantly influenced the design of numerous metasurfaces for optical vortex generation, each exhibiting unique functional advantages based on their underlying principles. Despite their innovative aspects, these designs are confronted with intrinsic limitations, notably

---

\* dkzhang@buaa.edu.cn

in the realm of nanoscale structural fabrication precision and the stringent specifications for polarization control. The geometric phase and the dynamic phase exhibit distinct correlations with the geometric configuration of the metasurface. Adjusting the nano units' dimensions and orientation creates a hybrid phase, offering potential to expand design limits and achieve significant advancements [25–27]. Considering that structural modifications influence both phases, precise dimension control is key in developing hybrid phases [28]. Therefore, elucidating the underlying correlations is essential for the optimization of such designs.

In this paper, we initially detail the methodology for delineating the dynamic and geometric phases introduced by metasurfaces. Thereafter, we engage in a quantitative analysis of the respective contributions of these phases to the generation of vortex beams, leveraging the combination of these two phases. Building upon these analyses, we engineer the metasurface structure to produce identical vortex beams through varied designs, and ultimately validate our theoretical concepts and design innovations through experimental verification. Through the synergistic integration of geometric and dynamic phases, we are able to design metasurfaces that exhibit enhanced flexibility and augmented functionality in the context of optical vortex generation. This advancement lays the groundwork for the development of innovative metasurface designs that incorporate a variety of materials and novel micro-nanostructures, thereby significantly benefiting the performance and capabilities of a multitude of optical devices.

## II. RESULTS AND DISCUSSION

### A. Dynamic and geometric phases

Firstly, we examine the methodologies for introducing two distinct types of phase shifts. Let  $|a\rangle$  represent the input polarized light state; upon interaction with the metasurface, this light is transformed into the output polarized state  $|b\rangle$ , as illustrated in Fig. 1(a). In accordance with the Pancharatnam connection, the phase shift between this two states can be indicated as  $\psi_{a \rightarrow b} = \arg(\langle a|b\rangle)$  [20]. We can use Jones matrix  $\mathbb{J}$  to represent optical elements, so the transformation process can be described as  $|b\rangle = \mathbb{J}|a\rangle$ . Assuming the  $2 \times 2$  matrix  $\mathbb{J}$  has two orthogonal eigenpolarization states  $|q_1\rangle, |q_2\rangle$  and the corresponding eigenvalues  $\mu_1, \mu_2$ . This implies that, for input light with eigenpolarization  $|q_{1,2}\rangle$ , the metasurface imparts a normalized transmittance of  $|\mu_{1,2}|$  and a phase shift of  $\arg(\mu_{1,2})$ , constituting the eigen-responses. Generally, the phase shift  $\psi_{a \rightarrow b}$  between the input  $|a\rangle$  and the output  $|b\rangle$  can be divided into two components,

$$\psi_{a \rightarrow b} = \psi_D + \psi_{PB}, \quad (1)$$

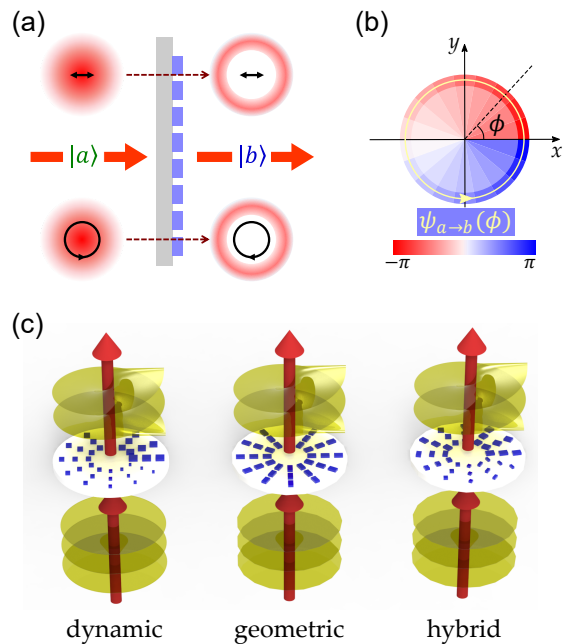


Figure 1. Optical vortex beams generated using metasurfaces. (a) A Gaussian distributed planewave ( $|a\rangle$ ) passes through metasurface chip and is converted into a scalar vortex beam ( $|b\rangle$ ) with doughnut-like intensity distribution. (b) The spiral phase profile is generated by the metasurface for the transformation from  $|a\rangle$  to  $|b\rangle$ . (c) Left: Generating vortices with dynamic phase gradient by varying the nano units size of metasurface. Center: Generating vortices with geometric phase gradient by rotating the nano units orientation for metasurface. Right: Generating vortices with hybrid phase gradient by adjusting the size and orientation of nano units.

where  $\psi_D$  denotes the dynamic phase and  $\psi_{PB}$  is named as the geometric phase, also known as the Pancharatnam-Berry (PB) phase [19, 20, 29]. For a lossless conversion, there is  $\psi_D = \arg(\mu_1\mu_2)/2$ , indicating the expected dynamic phase that the beam acquires upon transmission through the metasurface. Further,  $\psi_{PB}$  can be given by

$$\psi_{PB} = \arg[\cos \psi_- + i \sin \psi_- \exp(i\psi_{qa})], \quad (2)$$

where  $\psi_- = \arg(\mu_1\mu_2^*)/2$  and  $\psi_{qa} = \arg(\mathbf{Q} \cdot \mathbf{A})$  with  $\mathbf{Q}$  and  $\mathbf{A}$  are the Stokes vectors corresponding to  $|q_1\rangle$  and  $|a\rangle$ , and the detailed deduction can be found in Supporting Information. Owing to the inclusion of the  $\mathbf{Q} \cdot \mathbf{A}$  term,  $\psi_{PB}$  is associated with both the eigenstate of the metasurface and the polarization state of the input light. Figure 2(a) illustrates this relationship by depicting the phase shifts on the complex plane.

For the generation of an OAM light beam utilizing metasurfaces, a spiral phase shift along the azimuthal angle  $\phi$  is necessitated. As shown in Fig. 1(b), the phase shift  $\psi_{a \rightarrow b}(\phi)$  facilitates the generation of a vortex beam, wherein the OAM charge is associated with the gradient  $\partial\psi_{a \rightarrow b}/\partial\phi$ . According to equation (1), the total OAM

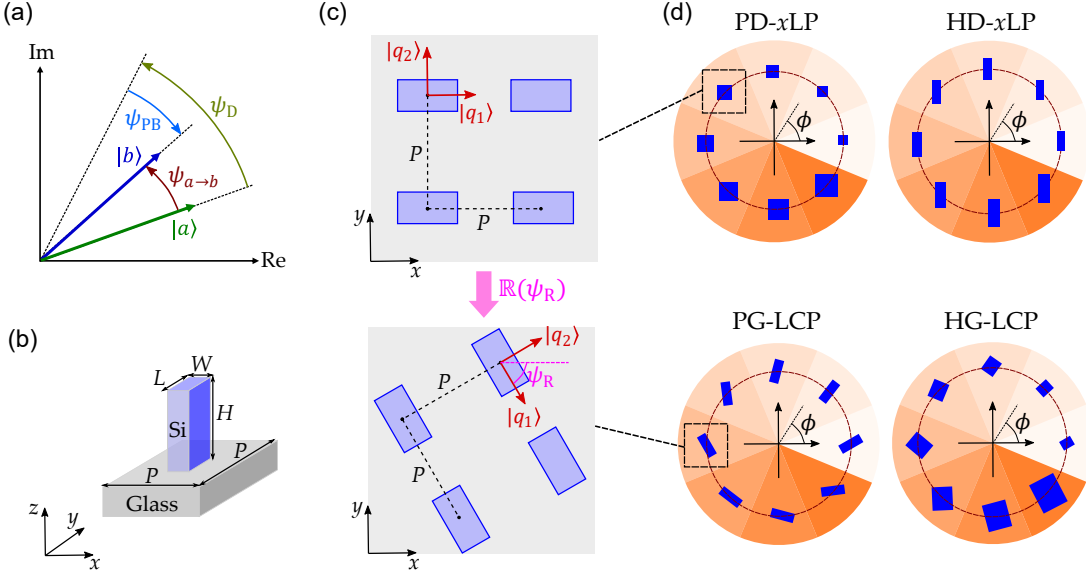


Figure 2. Phase shifts and configurations of metasurface. (a) Phase shifts from  $|a\rangle$  to  $|b\rangle$  induced by metasurface. (b) A nano-unit of the metasurface. (c) A uniform metasurface is achieved utilizing a standard arrangement (upper) and an alternate, rotated arrangement (lower). (d) Four metasurface designs, each based on an eight-sector configuration, are engineered to generate scalar vortex beams. The upper pair of metasurfaces is engineered to convert  $x$ -polarized light, while the lower pair is designed to transform LCP light.

charge, denoted as  $C_{\text{Tot}}$ , can be bifurcated into two components: the dynamical contribution ( $C_D \propto \partial\psi_D/\partial\phi$ ) and the geometrical contribution ( $C_{PB} \propto \partial\psi_{PB}/\partial\phi$ ), thereby establishing the relationship  $C_{\text{Tot}} = C_D + C_{PB}$  [30, 31]. Using equation (1), by maintaining  $\psi_{PB}$  as a constant value, we can achieve a pure dynamic phase gradient by adjusting  $\arg(\mu_1\mu_2)$ . This approach is termed the pure-dynamic design methodology. Alternatively, by sustaining  $\psi_D$  as a constant value, we can accomplish a pure geometric phase gradient by varying  $\psi_{PB}$ . This variation can be achieved by modulating  $\arg(\mu_1\mu_2^*)$  and  $\arg(\mathbf{Q} \cdot \mathbf{A})$  as prescribed by equation (2). This methodology for vortex beam generation epitomizes the pure-geometric design approach. In practice, the total phase gradient can be actualized by concurrently modulating  $\psi_D$  and  $\psi_{PB}$  along  $\phi$ , integrating the dynamical and geometrical contributions. This approach, which amalgamates both phase components, can be denoted as the hybrid design methodology.

## B. General description for lossless metasurfaces

As a fully polarized light beam traverses metasurface structures, the specific nano-unit and its corresponding array induce a definitive phase shift. The configuration of distinctly structured nano units within an array can induce varying phase shifts. Consequently, a proper design of the nano-unit combined with the strategic arrangement of the array can generate a spiral phase distribution across the transverse plane. For a lossless-transmission metasurface featuring nanofin arrays in the  $x-y$  plane, as shown in Fig. 2(b) and the upper panel of Fig. 2(c), there generally exist  $x(y)$ -polarized eigenstates denoted by  $[1, 0]^T$  and  $[0, 1]^T$ . The corresponding eigenvalues as  $\mu_{1,2} = \exp(i\varphi_{x,y})$ , where  $\varphi_{x,y}$  is the introduced phase shift for  $x(y)$ -polarized light by the nano-unit. Moreover, when a rotation angle  $\psi_R$  is imposed on the array (see Fig. 2(c)), the eigenstates associated with the nano-unit will be transformed to  $|q_1\rangle = \mathbb{R}(\psi_R)[1, 0]^T$  and  $|q_2\rangle = \mathbb{R}(\psi_R)[0, 1]^T$ , where  $\mathbb{R}$  is the two-dimensional rotation matrix. For this rotated nano-unit, the Jones matrix  $\mathbb{J}$  can be expressed as

$$\mathbb{J} = e^{i\psi_D} \begin{bmatrix} \cos\left(\frac{\psi_B}{2}\right) + i \sin\left(\frac{\psi_B}{2}\right) \cos(2\psi_R) & i \sin\left(\frac{\psi_B}{2}\right) \sin(2\psi_R) \\ i \sin\left(\frac{\psi_B}{2}\right) \sin(2\psi_R) & \cos\left(\frac{\psi_B}{2}\right) - i \sin\left(\frac{\psi_B}{2}\right) \cos(2\psi_R) \end{bmatrix} \quad (3)$$

where  $\psi_D = (\varphi_x + \varphi_y)/2$  is the introduced dynamic phase

and  $\psi_B = \varphi_x - \varphi_y$  denotes the birefringent phase differ-

ence between transmissions of the two eigenstates [26, 30]. Building upon the preceding discussion, there are three methodologies to accomplish the spiral phase profile for the generation of scalar vortex beams. In the generations, the dynamic contribution to the OAM charge is associated with  $\partial\psi_D/\partial\phi$ , whereas the geometric contribution, represented by  $\partial\psi_{PB}/\partial\phi$ , is linked to both  $\psi_B(\phi)$  and  $\psi_R(\phi)$ , since  $\psi_- = \psi_B/2$  and  $\mathbf{Q} \cdot \mathbf{A}$  depends on the rotated eigenstates  $|q_1\rangle$ .

In the pure-dynamic design approach utilizing metasurfaces, it is imperative to maintain the birefringent phase difference at a constant value. A prevalent strategy involves employing structures characterized by circular symmetry, such as cylinders or circular holes [32], to ensure that  $\psi_B = 0$ . For the unit founded on a nanofin structure with  $C_2$  symmetry, it is feasible to fine-tune  $\mu_1$  and  $\mu_2$  by modulating the dimensions of  $W$  and  $L$  (see Fig. 2(b)). In order to realize  $\psi_B = 0$ , squared nanofins (with  $C_4$  symmetry) are employed to induce an identical phase shift in both eigen-responses. Furthermore, by maintaining  $\psi_R(\phi)$  as a constant,  $\arg(\mathbf{Q} \cdot \mathbf{A})$  becomes fixed, resulting in  $C_{PB} = 0$ . Subsequently, imposing a spiral profile on  $\psi_D(\phi)$  by adjusting  $\varphi_x + \varphi_y$  of the nano-unit is required. The OAM charge generated is determined solely by  $C_{Tot} = C_D$ .

For the pure-geometric design approach, by maintaining  $\psi_D$  and  $\psi_-$  fixed as constants, we can manipulate the orientation of the nano units to modify the value of  $\arg(\mathbf{Q} \cdot \mathbf{A})$ , thereby achieving pure PB-phase metasurfaces. This approach facilitates the generation of phase gradients without altering the dimensions of the nano units, accomplished solely by adjusting the orientation angle [33–35]. This technique is straightforward and commonly employed in the design of geometric phase metasurfaces. Specially, when  $\psi_-$  equals to  $\pi/2$  (i.e.,  $\psi_B = \pi$ ) and the input light is circularly polarized, the resultant output is also a circularly polarized light with the opposite chirality. In this transformation, we can derive a relationship where  $\psi_{a \rightarrow b} = 2\psi_R$ . This straightforward link facilitates the extensive utilization of circularly polarized light as an ideal input for PB-phase based metasurfaces. For the nano-unit equipped with a nanofin, particular dimensions can be chosen to set  $\psi_B = \pi$ , followed by rotating the nano-unit to induce a phase gradient along  $\phi$ . The resulting OAM charge can be attributed  $C_{Tot} = C_{PB} = 2\partial\psi_R/\partial\phi$ .

To demonstrate the efficacy of the hybrid design approach, our objective is to achieve an equivalent outcome: generating an identical vortex beam for a specified input light. In this study, we conducted two hybrid design comparisons against the conventional pure-dynamic and pure-geometric designs, respectively. For the pure-dynamic designed metasurface, the total phase gradient  $\partial\psi_{a \rightarrow b}/\partial\phi$  is solely derived from the dynamic phase profile  $\psi_D(\phi)$ . For comparative purposes, in the hybrid design, we diminish  $\partial\psi_D/\partial\phi$  while enhancing  $\partial\psi_{PB}/\partial\phi$  to maintain a constant  $\partial\psi_{a \rightarrow b}/\partial\phi$ . This design requirement can be readily fulfilled by meticulously adjusting  $\varphi_x + \varphi_y$  and  $\varphi_x - \varphi_y$  along  $\phi$ , while ensuring  $\psi_R(\phi) = 0$ . Similarly,

for the pure-geometric designed metasurface, the phase gradient  $\partial\psi_{a \rightarrow b}/\partial\phi$  is entirely produced by the geometric phase profile  $\psi_{PB}(\phi)$ . For comparative analysis, we can diminish  $\partial\psi_{PB}/\partial\phi$  and augment  $\partial\psi_D/\partial\phi$  to maintain a constant  $\partial\psi_{a \rightarrow b}/\partial\phi$  in the hybrid design. This manipulation can be accomplished by concurrently adjusting  $\varphi_x + \varphi_y$  and  $\psi_R$  along  $\phi$ , with  $\varphi_x - \varphi_y$  set to  $\pi$ .

### C. Design and simulation

In our demonstration, the unit structure is made of a silicon nanofin on a glass substrate, as shown in Fig. 2(b). In order to determine the eigen-responses of the nano unit array, we employ the Rigorous Coupled-Wave Analysis (RCWA) to compute the transmitted eigen-responses of periodic array structures upon the incidence of  $x$ - and  $y$ -polarized plane waves. In our design and simulation, the pitch of the nano units was maintained at 400 nm in both directions. With a nanofin height of 400 nm, by varying the width ( $W$ ) and length ( $L$ ) of nanofin, the simulated  $x$ -polarized eigen-responses of  $\varphi_x$  and  $t_x$  are displayed in Figs. 3(a) and 3(b), respectively. These two parameters respectively denote the phase shift and trans-

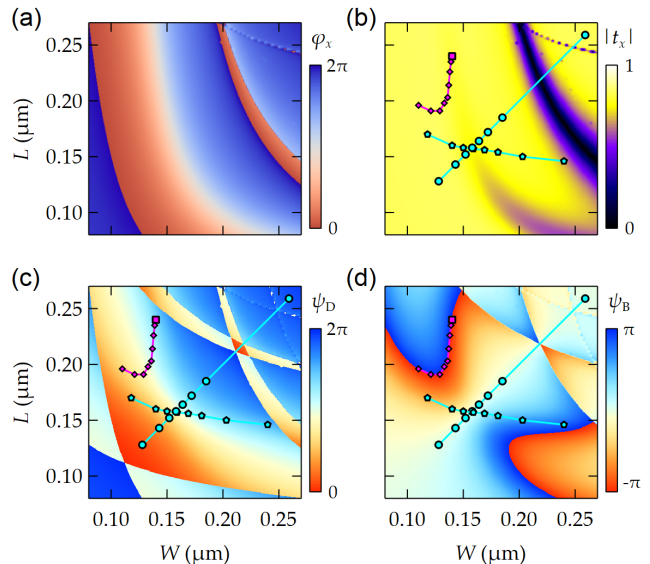


Figure 3. Basic optical features of uniform metasurfaces. (a) The phase shift  $\varphi_x$  and (b) transmittance  $t_x$  exhibit dependencies on the nanofin dimensions ( $W$ ,  $L$ ) for  $x$ -polarized light upon transmission through a uniform metasurface. The  $y$ -polarized responses can be obtained by exchanging the axes of  $W$  and  $L$  in (a) and (b). Upon calculating the phase shifts for  $x$ - and  $y$ -polarized lights, (c) the dynamic phase  $\psi_D$  and (d) the birefringent phase difference  $\psi_B$  are determined and illustrated. In (b-d), the eight circular markers correspond to parameters of PD- $x$ LP, while the eight pentagonal markers denote parameters of HD- $x$ LP. The square marker indicates parameters for PG-LCP, and the eight diamond markers signify parameters for HG-LCP.

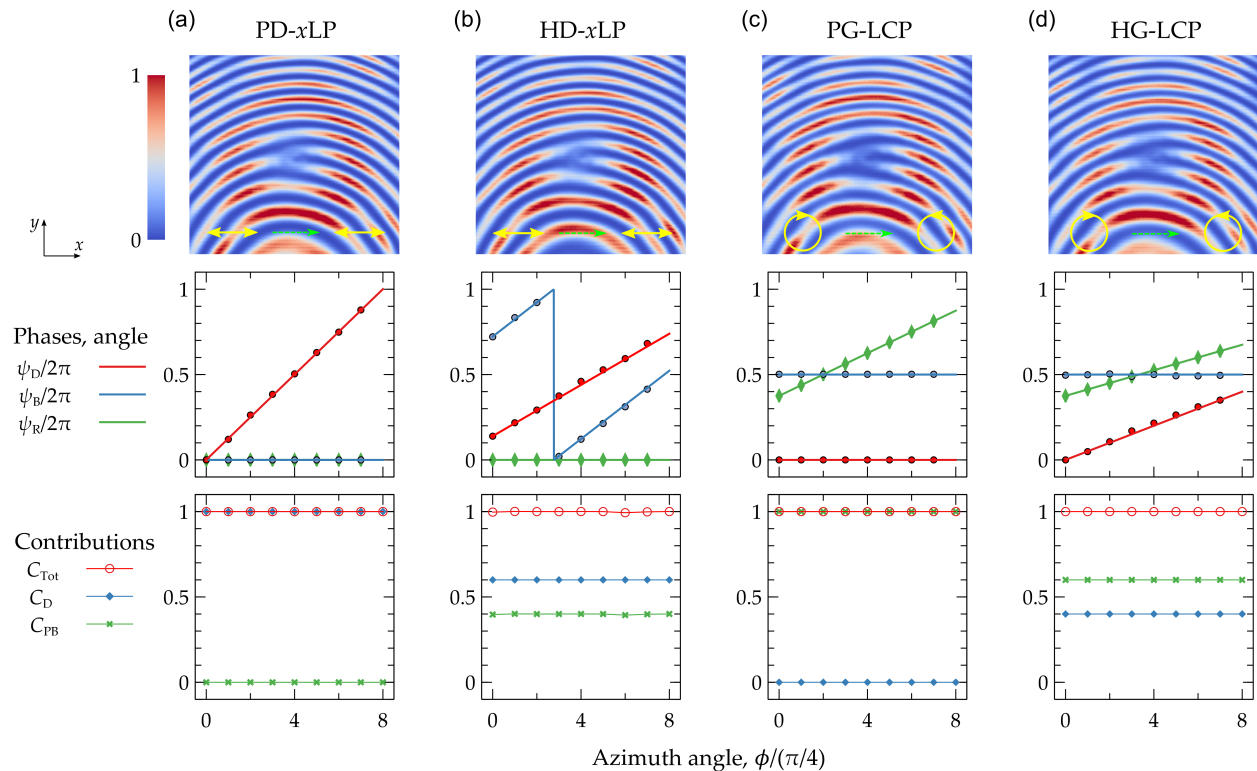


Figure 4. Four distinct metasurface configurations are engineered to produce optical vortex beams. Metasurfaces utilizing (a) pure-dynamic phase and (b) hybrid phase to convert an  $x$ -polarized plane wave to an  $x$ -polarized vortex beam. Metasurfaces employing (c) pure-geometric phase and (d) hybrid phase to convert a LCP plane wave to a RCP vortex beam. For (a-d), the first row displays the calculated interference patterns between a conventional Gaussian beam and the generated vortex beam, where there is a shift between the centers of two beams, under the ideal predefined incident polarization. There is a displacement between the centers of the two beams in the interference. The second row presents the designed phase set  $\{\psi_D, \psi_B, \psi_R\}$  of the nano-unit relative to the azimuth angle. Here, solid lines represent the desired values, while the marked points indicate the actual values of the selected nano-unit in each of the eight sectors. The third row illustrates the contributions of the two types of phase gradients to the OAM charge.

mittance experienced by  $x$ -polarized light upon passing through a uniform array. Owing to the  $C_2$  symmetry of the nanofin, the  $y$ -polarized eigen-responses of  $\varphi_y$  and  $t_y$  can be easily determined by merely switching the coordinate axes in Figs. 3(a) and 3(b). Utilizing the simulated maps of  $\varphi_x$  and  $\varphi_y$ , the corresponding maps for  $\psi_D$  and  $\psi_B$  are derived and displayed in Figs. 3(c) and 3(d), respectively. To generate vortex beams, a spiral spatial phase profile must be incorporated into the cross-section that is orthogonal to the direction of propagation. In our experimental demonstrations, the spiral phase profile is constructed by segmenting the structure into eight sectors along the azimuthal angle  $\phi$ , each characterized by discrete phase increments, as shown Fig. 2(d). Within each sector, a uniform array of nano units is meticulously arranged to facilitate the desired phase shifts. To approximate a lossless condition, all nano units are chosen for their high transmittance.

As described previously, we will undertake four metasurface designs to produce scalar vortex beams with an OAM charge of 1. The first design, denoted as PD- $x$ LP,

involves the generation of a pure-dynamic vortex beam. In this case, the sampled  $\psi_D(\phi)$  values for the eight sectors are incrementally increased, while  $\psi_B(\phi)$  is set to 0 for all nano units without any rotation, ensuring that  $\psi_R(\phi) = 0$ . In comparison, the hybrid design referred to as HD- $x$ LP integrates the spiral phase by sampling both  $\psi_D(\phi)$  and  $\psi_B(\phi)$ , applying incremental steps to the nano units across the eight sectors, while  $\psi_R(\phi)$  is maintained at 0. The schematics for both designs are presented in the first row of Fig. 2(d). Both of PD- $x$ LP and HD- $x$ LP designs have the capability to convert an  $x$ -polarized plane wave into a scalar vortex beam with an OAM charge of 1. The pure-geometric design, denoted as PG-LCP, is illustrated for converting a LCP plane wave into a vortex beam with the opposite polarization chirality. The gradient of geometric phase is accomplished by rotating the uniform nano-units, which have  $\psi_B(\phi) = \pi$ , to different angles  $\psi_R(\phi)$  within each sector. For comparison, the hybrid design, denoted as HG-LCP, is implemented by incorporating varied  $\psi_D(\phi)$  through the adjustment of eight nano-unit structures, while maintaining  $\psi_B(\phi) = \pi$ .

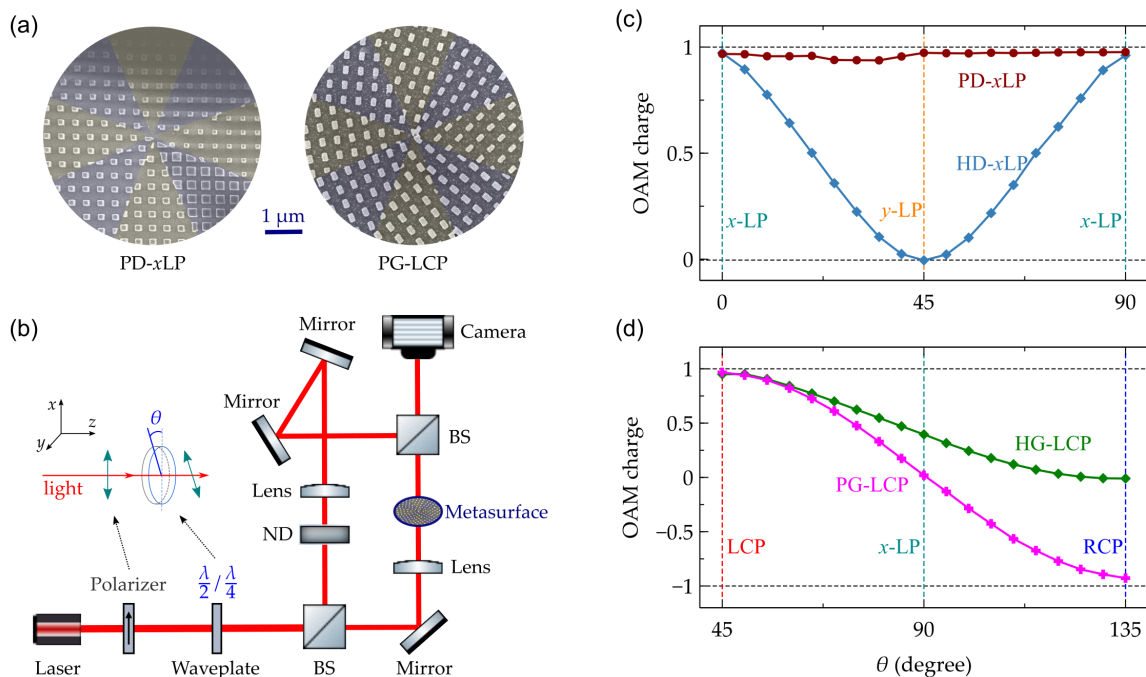


Figure 5. Fabricated metasurfaces and measurement setups. (a) Scanning electron microscope (SEM) images of the fabricated samples of PD- $x$ LP and PG-LCP designs. (b) The proposed measurement apparatus for the optical vortex beams produced by the designed metasurfaces relies on the interference of a reference beam with the generated vortex beam to yield the interference pattern. The beam splitter (BS) facilitates either the division or combination of light beams, while the neutral density filter (ND) is utilized to equilibrate the powers of the two beams, ensuring prominent interference fringes. The inset illustrates a polarizer accompanied by a  $\lambda/2$  ( $\lambda/4$ ) waveplate, employed to alter the polarization state of the incident light. (c) The average OAM charge of optical vortex beams generated by PD- $x$ LP and HD- $x$ LP designs is calculated and graphically represented at different directions of incident linear polarizations, which are adjusted using the polarizer and the rotated  $\lambda/2$  waveplate. (d) The average OAM charge of vortex beams produced by PG-LCP and HG-LCP designs is computed and plotted at distinct incident polarization states (from LCP to RCP), which are modified using the polarizer and the rotated  $\lambda/4$  waveplate.

The illustrations of the two designs are presented in the second row of Fig. 2(d). Both the PG-LCP and HG-LCP designs have the capability to convert an LCP plane wave into an RCP vortex beam with an OAM charge of 1.

Taking these considerations into account, the dimensions of the nanofins for the four designs are selected and marked in Figs. 3(b-d). The corresponding set of  $\{\psi_D, \psi_B, \psi_R\}$  for each nano-unit are summarized and plotted in the middle panels of Figs. 4(a-d) for the four designs, respectively. Furthermore, the contributions for the OAM charge can be evaluated and displayed in the bottom panels of Figs. 4(a-d). With the simulation results of each nano-unit shown in Figs. 3(a-d), the transformed far field can be calculated with the corresponding input light beams. To confirm the OAM charge of the generated vortices, the simulated interference patterns of the vortex beams with a conventional Gaussian beam are displayed in the top panels of Figs. 4(a-d). The superposition of a vortex beam and a plane wave results in an interference pattern characterized by a fork-like bifurcation at the vortex core [36]. The specific morphology of this bifurcation is correlated with the OAM charge of the beam. As patterns shown in Figs. 4(a-d), the red-colored toroidal

contour is a distinctive characteristic of vortex beams, with a fork-shaped pattern at the center, featuring two distinct branches that signify an OAM charge of 1.

#### D. Experimental results

The designed samples were fabricated using a borosilicate glass substrate with a thickness of 1 mm, followed by the evaporation of a 400 nm silicon film. Subsequently, silicon nanofins were patterned within a 0.5 mm diameter circle through electron-beam lithography and a dry etching process. Figure 5(a) shows scanning electron microscope (SEM) images of two fabricated samples corresponding to the PD- $x$ LP and PG-LCP designs. A Mach-Zehnder interferometric system, constructed for characterization purposes, is illustrated in Fig. 5(b). The light beam is produced by a laser with a wavelength of 780 nm and is adjusted to  $x$ -polarized light using a polarizer. Subsequently, a half-wave ( $\lambda/2$ ) or quarter-wave ( $\lambda/4$ ) waveplate is employed to transform the  $x$ -polarized light into linearly, elliptically, or circularly polarized light. The light beam is subsequently split into two, with one portion passing

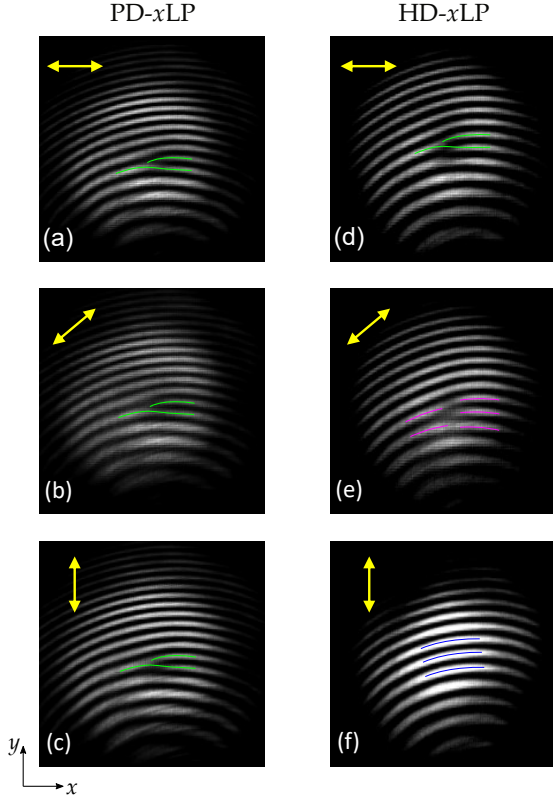


Figure 6. Measured interference patterns for optical vortex beams generated by PD- $x$ LP and HD- $x$ LP metasurfaces at different directions of incident linear polarizations: (a,d)  $x$ -polarized, (b,e)  $45^\circ$  linearly polarized, and (c,f)  $y$ -polarized.

through the metasurface chip. These two beams are ultimately recombined, generating interference patterns that are captured by a charge-coupled device (CCD) camera. As shown in the inset of Fig. 5(b), by changing the angle  $\theta$  between the optical axes of polarizer and  $\lambda/2$  (or  $\lambda/4$ ) waveplate, any desired linearly polarized (or circularly polarized) light can be obtained. Utilizing these polarization modifications, we are able to confirm the production of vortex beams induced by the metasurfaces and further assess the reliance of various metasurfaces on the polarization states of the incident light.

In the configuration involving the polarizer and the  $\lambda/2$  waveplate, the orientation of linear polarization undergoes a rotation of  $2\theta$  corresponding to the rotation  $\theta$  of the  $\lambda/2$  waveplate. For the pure-dynamic metasurface (PD- $x$ LP), the rotation of the  $\lambda/2$  waveplate exerts a minimal impact on the outcomes, which is consistent with its polarization-independent properties, as shown in Fig. 5(c). The light field and OAM charge of the generated vortex beams remain unaffected by the polarization state of the input light, with their interference fringes displayed in Figs. 6(a-c). In the case of the hybrid design (HD- $x$ LP), a distinct polarization dependence is observed, as illustrated by the calculated OAM charge shown in Fig. 5(c). An optimal vortex beam is generated when the incident light is  $x$ -

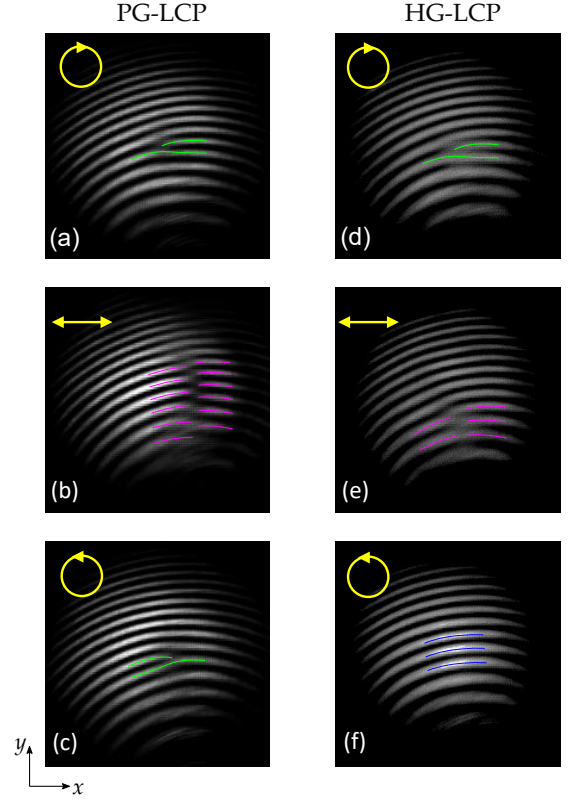


Figure 7. Measured interference patterns for optical vortex beams generated by PG-LCP and HG-LCP metasurfaces at different incident polarization states: (a,d) LCP, (b,e)  $x$ -polarization, and (c,f) RCP.

polarized. When the incident light is  $y$ -polarized, the output remains a planewave, and the interference fringes manifest as alternating bright and dark stripes. These findings are confirmed by experimental results presented in Figs. 6(d-f) (also see Supporting Information). It is crucial to highlight that, for both the PD- $x$ LP and HD- $x$ LP designs, identical vortex beams can be produced using  $x$ -polarized incident light.

Typically, the geometric phase exhibits high sensitivity to the polarization state of the incident light. As the light traverses the polarizer and the  $\lambda/4$  waveplate, its polarization can be transformed into linear, elliptical, or circular polarization, depending on the rotation  $\theta$  of the  $\lambda/4$  waveplate. According to the calculations illustrated in Fig. 5(d), the OAM charge of the pure-geometric design (PG-LCP) is heavily reliant on the polarization state of light. Specifically, the sign of the OAM charge is inverted for input light of opposite chirality, reflecting the conjugate symmetry inherent in the relationship between the input and output fields. From the interference fringes shown in Figs. 7(a) and 7(c), it is observed that input light of distinct chiralities results in the formation of interference fringes oriented in opposite directions. However, upon linear polarization of the input light, the output light undergoes transformation into a vector vortex beam

(see Supporting Information). Upon interference with circularly polarized reference light, an interlaced pattern of interference fringes is theoretically produced and the experimental result is shown in Fig. 7(b). In the case of the hybrid design (HG-LCP), the OAM charge of the output light remains associated with the incident polarization state (see Fig. 5(d)). Nevertheless, compared to the pure geometric design, the fluctuation in the OAM charge is attenuated, and no distinct reversal is observed. Experimental findings suggest that a well-defined vortex beam is exclusively produced when the input light possesses an LCP state (see Fig. 7(d)). Conversely, employing RCP light results in an output light with a negligible topological charge, culminating in an interference pattern characterized by alternating bright and dark stripes (see Fig. 7(f)). Consequently, both the PG-LCP and HG-LCP metasurfaces are capable of executing identical transformations for LCP input light. However, the extent of reliance on the incident polarization state varies, as the dynamic contribution within the hybrid design can effectively mitigate polarization dependence.

In this study, we showcased that metasurfaces with various designs can produce scalar vortex beams. For a particular transformation, aside from the conventional methods employing pure-dynamic or pure-geometric generation of the spiral phase profile, there exists substantial potential in designs that integrate both dynamic and geometric contributions. These hybrid designs can overcome certain constraints regarding the choice of materials and forms for nano-units. Furthermore, transformations based on hybrid designs offer distinct advantages: In the case of a pure-dynamic design, there is no selectivity towards the polarization state of the input light. However, the hybrid design can introduce a polarization filter, and its sensitivity or bandwidth can be customized by adjusting the geometric contribution. Conversely, the pure-geometric design mandates a stringent requirement for the polarization state of the input light; however, this constraint can be alleviated in the hybrid design by incorporating the dynamic contribution. In the experiment, we successfully generated a vortex beam with an OAM charge of 1. However, there are no constraints on producing higher-order optical vortices using hybrid designs; this can be accomplished by expanding the number of sampling sectors and enhancing the requisite phase gradient.

Besides generating scalar vortex beams, hybrid designs offer the advantage of producing vector vortices, thanks to the incorporated geometric contributions.

### III. CONCLUSION

Metasurfaces can yield dynamic and geometric phases, both of which are extensively employed to produce optical vortex beams. However, in reality, by leveraging the combined dynamic and geometric phases, innovative and diverse functionalities can be realized in the engineering of optical vortex beam generation. In this study, the spiral phase distribution is achieved through the customization of hybrid phases to produce scalar vortex beams. Additionally, the OAM contributions from the two phases can be precisely apportioned. Utilizing metasurfaces that incorporate hybrid phases, we introduce an optimization strategy for the engineering of nano units, addressing both structural and functional dimensions. The hybrid design concept we introduce is not restricted by the material, structure, or propagation manner of metasurfaces. This principle opens up the possibility of employing hybrid phases to engineer a variety of phase profiles that can facilitate new functionalities and pave the way for innovative optical devices in the future.

#### Funding

This work is supported by the Fundamental Research Funds for the Central Universities under Grant KG21008401.

**Disclosures.** The authors declare no competing financial interests.

**Data availability.** Data underlying the results presented in this paper are not publicly available at this time but may be obtained from the authors upon reasonable request.

**Supporting Information.** Detailed theoretical derivation of phase components, simulated transformations of the polarization state from input to output, and experimental far-field patterns of vortex beams and interference fringes at varying input polarization states.

- 
- [1] Dennis, M. R., O’Holleran, K. & Padgett, M. J. Singular optics: Optical vortices and polarization singularities. *Prog. Opt.* **53**, 293–363 (2009).
  - [2] Shen, Y. *et al.* Optical vortices 30 years on: OAM manipulation from topological charge to multiple singularities. *Light: Sci. Appl.* **8**, 90 (2019).
  - [3] Molina-Terriza, G., Torres, J. P. & Torner, L. Twisted photons. *Nat. Phys.* **3**, 305–310 (2007).
  - [4] Franke-Arnold, S., Allen, L. & Padgett, M. J. Advances in optical angular momentum. *Laser Photonics Rev.* **2**, 299–313 (2008).
  - [5] Bliokh, K. Y. & Nori, F. Transverse and longitudinal angular momenta of light. *Phys. Rep.* **592**, 1–38 (2015).
  - [6] Yao, A. M. & Padgett, M. J. Orbital angular momentum: origins, behavior and applications. *Adv. Opt. Photonics* **3**, 161 (2011).
  - [7] Miao, P. *et al.* Orbital angular momentum microlaser. *Science* **353**, 464–467 (2016).
  - [8] Zhang, Z. *et al.* Tunable topological charge vortex microlaser. *Science* **368**, 760–763 (2020).



- [9] Wang, X. *et al.* Recent advances on optical vortex generation. *Nanophotonics* **7**, 1533–1556 (2018).
- [10] Yu, N. *et al.* Light propagation with phase discontinuities: Generalized laws of reflection and refraction. *Science* **334**, 333–337 (2011).
- [11] Meinzer, N., Barnes, W. L. & Hooper, I. R. Plasmonic meta-atoms and metasurfaces. *Nat. Photonics* **8**, 889–898 (2014).
- [12] Kamali, S. M., Arbabi, E., Arbabi, A. & Faraon, A. A review of dielectric optical metasurfaces for wavefront control. *Nanophotonics* **7**, 1041–1068 (2018).
- [13] Yu, N. & Capasso, F. Flat optics with designer metasurfaces. *Nat. Mater.* **13**, 139–150 (2014).
- [14] Overvig, A. C. *et al.* Dielectric metasurfaces for complete and independent control of the optical amplitude and phase. *Light: Sci. Appl.* **8** (2019).
- [15] Bai, Y., Lv, H., Fu, X. & Yang, Y. Vortex beam: generation and detection of orbital angular momentum [invited]. *Chin. Opt. Lett.* **20**, 012601 (2022).
- [16] Zhang, Y., Liu, W., Gao, J. & Yang, X. Generating focused 3D perfect vortex beams by plasmonic metasurfaces. *Adv. Opt. Mater.* **6** (2018).
- [17] Wang, D. *et al.* High-efficiency metadevices for bifunctional generations of vectorial optical fields. *Nanophotonics* **10**, 685–695 (2020).
- [18] Guo, Y. *et al.* Classical and generalized geometric phase in electromagnetic metasurfaces. *Photonics Insights* **1**, R03 (2022).
- [19] Berry, M. The adiabatic phase and pancharatnam’s phase for polarized light. *J. Mod. Opt.* **34**, 1401–1407 (1987).
- [20] Gutiérrez-Vega, J. C. Pancharatnam-berry phase of optical systems. *Opt. Lett.* **36**, 1143 (2011).
- [21] Khorasaninejad, M. *et al.* Polarization-insensitive metalenses at visible wavelengths. *Nano Lett.* **16**, 7229–7234 (2016).
- [22] Bliokh, K. Y., Rodríguez-Fortuño, F. J., Nori, F. & Zayats, A. V. Spin-orbit interactions of light. *Nat. Photonics* **9**, 796–808 (2015).
- [23] Devlin, R. C., Ambrosio, A., Rubin, N. A., Mueller, J. P. B. & Capasso, F. Arbitrary spin-to-orbital angular momentum conversion of light. *Science* **358**, 896–901 (2017).
- [24] Marrucci, L., Manzo, C. & Paparo, D. Optical spin-to-orbital angular momentum conversion in inhomogeneous anisotropic media. *Phys. Rev. Lett.* **96**, 163905 (2006).
- [25] Arbabi, A., Horie, Y., Bagheri, M. & Faraon, A. Dielectric metasurfaces for complete control of phase and polarization with subwavelength spatial resolution and high transmission. *Nat. Nanotechnol.* **10**, 937–943 (2015).
- [26] Balthasar Mueller, J., Rubin, N. A., Devlin, R. C., Groever, B. & Capasso, F. Metasurface polarization optics: Independent phase control of arbitrary orthogonal states of polarization. *Phys. Rev. Lett.* **118**, 113901 (2017).
- [27] Zhang, S. *et al.* Dynamic display of full-stokes vectorial holography based on metasurfaces. *ACS Photonics* **8**, 1746–1753 (2021).
- [28] Wang, Z. *et al.* Bifunctional manipulation of terahertz waves with high-efficiency transmissive dielectric metasurfaces. *Adv. Sci.* **10** (2022).
- [29] Martínez-Fuentes, J. L., Albero, J. & Moreno, I. Analysis of optical polarization modulation systems through the pancharatnam connection. *Opt. Commun.* **285**, 393–401 (2012).
- [30] Zhang, D., Feng, X. & Huang, Y. Orbital angular momentum induced by nonabsorbing optical elements through space-variant polarization-state manipulations. *Phys. Rev. A* **98**, 043845 (2018).
- [31] Zhang, D., Feng, X., Cui, K., Liu, F. & Huang, Y. Identifying orbital angular momentum of vectorial vortices with pancharatnam phase and stokes parameters. *Sci. Rep.* **5**, 11982 (2015).
- [32] Sun, J. *et al.* Spinning light on the nanoscale. *Nano Lett.* **14**, 2726–2729 (2014).
- [33] Chen, M., Jiang, L. & Sha, W. Orbital angular momentum generation and detection by geometric-phase based metasurfaces. *Appl. Sci.* **8**, 362 (2018).
- [34] Huo, P. *et al.* Photonic spin-multiplexing metasurface for switchable spiral phase contrast imaging. *Nano Lett.* **20**, 2791–2798 (2020).
- [35] Karimi, E. *et al.* Generating optical orbital angular momentum at visible wavelengths using a plasmonic metasurface. *Light: Sci. Appl.* **3**, e167–e167 (2014).
- [36] Liu, G.-G. *et al.* Measurement of the topological charge and index of vortex vector optical fields with a space-variant half-wave plate. *Opt. Lett.* **43**, 823 (2018).